

# Disparity improvement of brain tissues after MRI segmentation in tDCS rehabilitation

Maryam Yousefian

Faculty of Electrical and Computer  
Engineering, University of Tabriz,  
Tabriz, Iran.

maryamyousefian95@ms.tabrizu.ac.ir

Ali Amani

Faculty of Electrical and Computer  
Engineering, University of Tabriz,  
Tabriz, Iran.

a.amani95@ms.tabrizu.ac.ir

Hadi Seyedarabi

Faculty of Electrical and Computer  
Engineering, University of Tabriz,  
Tabriz, Iran.

seyedarabi@tabrizu.ac.ir

Mehdi Farhoudi

Neurosciences Research Center  
(NSRC), Tabriz University of Medical  
Science, Tabriz, Iran.

farhoudim@tbzmed.ac.ir

**Abstract**— Segmentation of brain Magnetic Resonance Imaging (MRI) has a significant role in computational modeling of transcranial Direct Current Stimulation (tDCS); hence, it is important to choose the appropriate method that can be utilized with adequate precision. Some tissues such as Cerebrospinal fluid (CSF) and white matter (WM) usually get damaged after segmentation, because of their low thickness. This defect appears in the form of small cavities on their wall. So, it causes many problems in the modeling and processing of tDCS. The modified automated correction routine compensates the results error adequately. Accordingly, the improved masks make the complete head model without any discontinuities in the CSF and WM surfaces, and the electric field magnitudes after stimulation, illustrate this improvement effectively.

**Keywords**— Magnetic Resonance Imaging (MRI), Tissue segmentation, Denoising, Modified automated correction routine, transcranial Direct Current Stimulation (tDCS), Electric field.

## I. INTRODUCTION

MRI plays a crucial role in the detection of pathologies. From several years ago, segmentation of brain MRI was a fundamental problem. More recent investigations clarified the advancement of medical images devices. The possibility of brain MRI acquisition with high quality and brain tissue segmentation with high accuracy have been created by using powerful tools [1, 2]. In general, the brain is a collection of adjacent tissues which interact together simultaneously, and each of them has a particular anatomical function. More specifically, the human's brain includes five main tissues that are named skin, skull, gray matter (GM), CSF, and WM. Brain tissue segmentation is an important step in the analysis of brain diseases [3-5]. It also has important applications on tDCS due to building the homogeneous head model [6]. tDCS is a noninvasive and painless brain stimulation technique that delivered the weak current flow (usually 1mA) to compensate some brain disorders over time. Its positive effect has been proved about some diseases such as Stroke, Depression, and so forth [7, 8]. tDCS requires several simulation steps when

is done by using the computer. Firstly, it is tissue segmentation. Secondly, it is to make a head model by creating a 3D model of each tissue [9, 10]. Next, it is to design the proper electrodes and then they are placed on the head model. Finally, after the mesh processing and some minor steps, the head model is ready to go to the last step [11]. The last step is stimulation with certain conditions. In this step, the Laplacian equation is solved in each element of the mesh model, and Finite Element Model (FEM) procedure is become complete [12]. There are several MATLAB toolboxes to automate tDCS steps, but each of them has its limitations. Manual tracing method is another common method that doctors still use it [13]. But it has some problems such as time-consuming, individual visibility error, etc. Hence, a large number of researchers have been attracted by automated methods [14]. Statistical Parametric Mapping (SPM) is one of them. It is a useful MATLAB toolbox that is created by the Centre for Human Neuroimaging, United Kingdom [15]. Despite its extensive applications, it has some errors during the brain tissues segmentation. Previous work of researchers suggested the automated correction routine and used it after brain tissues segmentation [16]. Besides, noise is one of the fundamental concerns in brain MRI scans. Noise makes complicated the medical images analysis. It can appear in different forms in the image [17, 18]. Thus, denoising is an important pre-processing step. There are several different ways to denoising the images [19]. In this paper, automated MATLAB toolbox is used to remove noise effects [20, 21]. The focus of this paper is the improvement of brain tissues masks after segmentation. Due to having a complete and uniform surface, we used automated correction routine and applied some changes on it. After proper changes, we named it the modified automated correction routine. Our changes caused that the mentioned algorithm works better than before, and the electric field magnitudes after stimulation are increased. All results are presented both in the visually and numerically in the next sections.

## II. MATERIAL AND METHODS

### A. Subjects

The used data were received from the MIDAS website [22]. All participants were in a healthy condition, and all samples were acquired on a 3T MRI under standardized protocols [23]. All images are exhibited in the MetaImage format, and they can be loaded by any software that supports MetaImage. Medical Images often include different types of noise which can somewhat destroy them. Fig.1 illustrates the original noisy image in the first column, and the same image after denoising the middle column, and also the removed noise in the last column. We used eight MRI samples in our study and applied all the steps to them. We tried all levels in three different states. Firstly, we use the SPM result mask. Secondly, we use the main algorithm masks, and finally, we use modified algorithm masks. All numerical and visual results are presented in the result and discussion section.

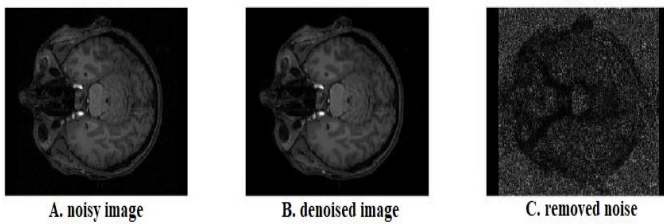


**Fig1.** Denoising procedure. A. Original noisy image B. Denoised image C. Removed noise

### B. The modified automated correction routine

Numerous small cavities appear on the CSF and WM output masks after segmentation, when using the SPM for segmentation. These cavities cause many problems in the next steps of tDCS. Hence, it is necessary to modify these tissues, and each tissue should have a uniform surface. The common errors that display after segmentation are divided into four general categories. First of them are unassigned voxels. They are the number of voxels that determine a zero probability to depend on tissues. The second problem is the disconnected voxels. They are disjoint voxels of particular tissue that erroneously place in the adjacent tissue. Next, it is the surface of CSF. It has a discontinuity surface after segmentation, while the CSF surface should be a continuous layer. The last error is the rough tissue masks. Sharpness can cause some problems. Therefore, smoothness can remove these sharp corners and makes a more realistic model. This algorithm uses the Gaussian filter with certain  $\sigma$ . This filter is intensively used in numerous research areas. This algorithm includes three free parameters. They are named smoothing length constant ( $s$ ), structural element size ( $x$ ), and threshold ( $N$ ). Smoothing length ( $s$ ) is to make the masks smoother; hence, gets the convergence and also decreases the size in the complete head model. The structural element size ( $x$ ) is to compensate the CSF discontinuities, and threshold ( $N$ ) is to identify the disconnected voxels [16]. The fundamental base of this algorithm is morphological and Boolean operations. All levels of the algorithm were implemented in MATLAB R2016b. In the modified automated correction routine, we add the mean filter to the main algorithm. Mean filter is one of the important linear filters that is utilized widely in image

processing. It replaces each value of pixels with the average value of their neighbors, including themselves. To apply this technique to all value of pixels in a certain image, it uses the kernels with different sizes. A  $3 \times 3$  square kernel is proper. We applied it to the CSF and WM that damaged after segmentation. Besides, different thresholds are considered in each tissue according to their specifications. Some of them work automatically; for instance, thresholds of the CSF and skin change with tissues volume, but some others are constant. We use different thresholds to get better results. This threshold eliminates the areas that the number of voxels is less than the threshold, and allocates its adjacent tissues. As previously mentioned, the CSF and WM are two important tissues, because there are many cavities on their surface after segmentation. After trial and error, we conclude that threshold=40 for GM and threshold=30 for WM create the best results. A critical factor that will be considered in the mentioned method, is sigma ( $\sigma$ ). Sigma magnitudes are considered equal to 0.1 in the main algorithm. But, we changed it. We examined different magnitudes and found the best value equal to 0.25. This can be a proper threshold for the modified algorithm. If this magnitude is more than 0.25, the result masks get blur. After calculating the maximum and average electric field, improvement on the electric field have been clearly observed. In the next section, results after these changes are entirely shown and completely discussed.

### C. Design and stimulation

In this section, several softwares are respectively have been used (Materialise Mimics 19.0., 3-matic Research 11.0, Simpleware Ltd, Exeter, UK, and COMSOL Inc., Burlington, MA), and then the tDCS steps has been completed. A complete 3D head model is made by Mimics, and electrode schemes are made by 3-matic and then they are placed on the scalp. Boolean operation and mesh processing are applied by Simpleware [14]. The stimulation process is applied by COMSOL Multiphysics, and the current flow with a certain amplitude (1mA) is applied to the anode, and the cathode becomes ground. The  $\nabla \cdot (\sigma \nabla V) = 0$  is considered with potential ( $V$ ) and conductivity ( $\sigma$ ), then it is solved for all elements that make a complete head model; namely, the Finite Element Method (FEM) is solved for a head model. All electrodes are considered as rectangular schemes with standard dimension equal to  $5 \times 7 \text{ cm}^2$ . In this research, we take six different electric parts with certain conductivities as below: air ( $1 \times 10^{-4} \text{ S/m}$ ), bone ( $1 \times 10^{-2} \text{ S/m}$ ), GM (0.276 S/m), CSF (1.65 S/m), skin (0.465 S/m), WM (0.126 S/m), and 2 S/m for desired electrodes [6].

## III. RESULTS

The modified automated correction routine was implemented for eight samples of healthy MRI. All images firstly denoised, and segmented then the mentioned algorithm applied for all of them. In Fig.2, the CSF and WM are systematically shown. They are segmented by the SPM for one of the samples.

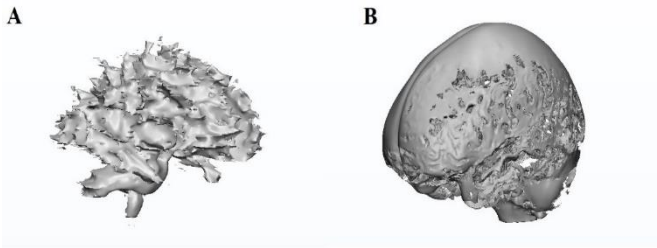


**Fig2.**The 3D model of CSF and WM after segmentation in SPM A. Discontinuities and cavities are observed on the surface of the WM. B. The CSF is observed before correction, with lots of cavities and discontinuities on it.

In Fig.3, the results are shown after performing a modified automated correction routine, and automated correction routine. In Fig.4, after performing of the mentioned algorithms, a mean volume of each five tissues for all eight samples are calculated.

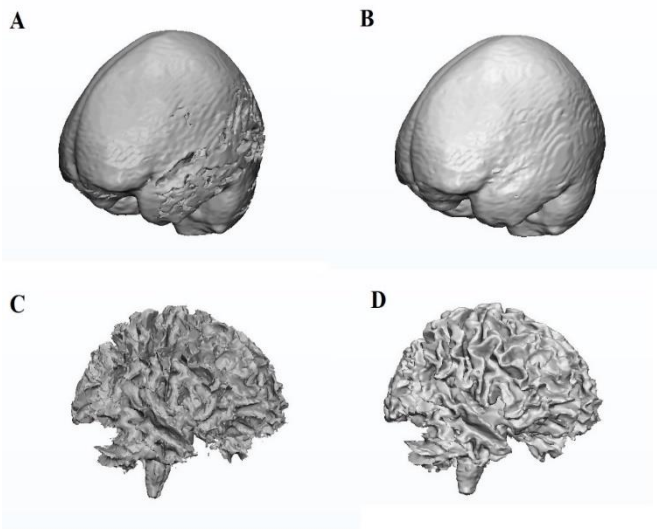


**Fig3.**The CSF and WM after the main algorithm and modified algorithm. It can be seen that cavities were filled and the segmented model has become complete A.CSF representation after the main algorithm, B.CSF representation after the modified algorithm, C.WM representation after the main algorithm, D.WM representation after the modified algorithm.

In Fig.5(a), electrode placement on the head model is shown before electric stimulation. In this Figure, an active electrode (anode) is placed on left Dorsolateral prefrontal cortex (DLPFC), and a return electrode (cathode) is placed on the Contralateral supraorbital area.

After stimulation, the electric field magnitudes with specific peak are shown by using the suitable toolbar in Fig 5(b). The average and maximum electric field were calculated for all eight samples, and the average quantities have been displayed. (See Table (1), and Table (2)).

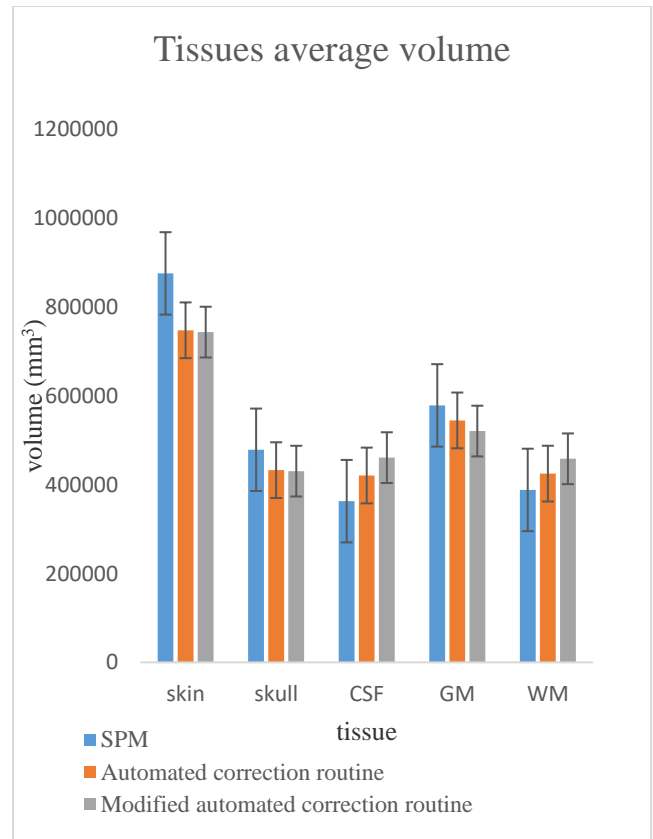


**Fig4.** This chart displays the mean volume of five segmented tissues in three different states.

**Table1.**The mean of maximum electric field ( $E_{max}$ ) after stimulation using three masks series for all samples (V/m).

Tissue type	SPM	Automated correction routine	Modified algorithm
CSF	0.42	0.48	0.53
WM	0.15	0.20	0.26
GM	0.32	0.34	0.38

**Table2.**The mean of average electric field ( $E_{ave}$ ) after stimulation using three masks series for all samples (V/m).

Tissue type	SPM	Automated correction routine	Modified algorithm
CSF	0.136	0.198	0.228
WM	0.042	0.069	0.076
GM	0.075	0.079	0.082

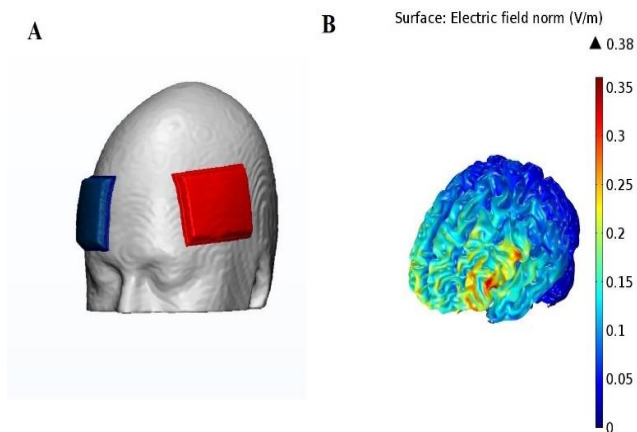


**Fig5.** A. A head model that electrodes were designed and placed on the skin. B. The electric field distribution on the GM.

#### IV. DISCUSSION

The principal novelty compared to the main proposed algorithm by other researchers, is the use of Mean filter to yield better results than before. Also, applying the proper change on the tunable parameters of the main algorithm is another suggestion. In general, each of these changes has caused the ultimate results are better than before. As can be seen from Fig.2, so many cavities are on the tissues wall, especially in CSF and WM. This defect appears more in the tissues with low thickness and can have different reasons. If these tissues are not corrected at this step, we will encounter some problems at the next steps. From Fig3, a remarkable improvement on the CSF and WM observes after a 3D modeling. Modification in the corrected tissues can be determined by comparing the volume of these tissues before and after the implementation of the algorithms. In Fig.4, it is clear that the volume of CSF and WM is increased than before. This indicates the filling of cavities and makes continues surface on the CSF and WM wall. After the tissue correction step, we used the results of this stage for making a head model in Mimics. In the next step, the electrodes were designed using 3-matic and were placed on the skin. The mesh processing was applied in the Simpleware. The final head model included 16 million small elements and the output file approximately had 850MB volume. The electric stimulation process with 1mA current flow was applied to the anode in the COMSOL Multiphysics. The electric field that was generated in different tissues, were calculated. From Table 1 and Table 2, we observed that the quantities of the maximum electric field have considerable changes than before, and also the average electric field have a slight changes. Hence, our applied changes have made better results than the results of main algorithm that is introduced by other researchers. Tissue correction makes the cavities to be filled. It connects the detached parts closely together and removes the small pieces away from tissues. It makes a complete head model. The effect of the above-mentioned procedures can be seen in Fig.3. By observing the results of Fig.4, it can be seen that the volumes of some tissues such as GM with more thickness has decreased. Also, results well show that the volume of some tissues with less thickness such as CSF and WM has increased after the correction. Applying the Mean filter automatically increases the thickness of tissues, but using proper boolean operation with adjacent tissues turns

them to previous states. Although some small parts of GM are removed while applying the boolean operation, it has not considerable changes on the final results. As shown in Table 1 and 2, after modifying automated correction routine in different tissues, the electric field has increased. These increased volume were predictable for WM and CSF because the main goal of the automated correction routine is to compensate for the CSF and WM defects after automated segmentation. Also, a slight electric field increase in GM is evident. This improvement in electric field results, related to the correction of adjacent tissues, makes better penetration of the current flow. Therefore, the concentration of the electric field is more. These results generally indicate the effectiveness of the modified automated correction routine, which was not predetermined. Both of them can cause better performance as the results show.

#### V. CONCLUSION

In conclusion, we should note that the main purpose of the current study was the improvement of the automated correction routine and then investigation of its effect on the electric field distribution in tDCS. This method has a crucial role in computational modeling due to having a complete head model. For this purpose, we applied two main steps. We utilized the mean filter appropriately, and then we considered suitable thresholds for some tissues in the mentioned algorithm. Also, we determined the proper sigma magnitude of the Gaussian filter, which had not been examined before. These changes show better electric field distribution results after stimulation on tested samples.

#### ACKNOWLEDGMENT

This work was supported by Iran Cognitive Sciences and Technologies Council (Project 4547). The brain MRI from healthy volunteers used in this paper were collected and made available by the CASILab at The University of North Carolina at Chapel Hill and were distributed by the MIDAS Data Server at Kitware, Inc.

#### REFERENCES

- [1] T. Kapur, W. E. L. Grimson, W. M. Wells III, and R. Kikinis, "Segmentation of brain tissue from magnetic resonance images," *Medical image analysis*, vol. 1, no. 2, pp. 109-127, 1996.
- [2] L. Lenchik et al., "Automated Segmentation of Tissues Using CT and MRI: A Systematic Review," *Academic radiology*, 2019.
- [3] D. T. Chard, G. J. Parker, C. M. Griffin, A. J. Thompson, and D. H. Miller, "The reproducibility and sensitivity of brain tissue volume measurements derived from an SPM - based segmentation methodology," *Journal of Magnetic Resonance Imaging: An Official Journal of the International Society for Magnetic Resonance in Medicine*, vol. 15, no. 3, pp. 259-267, 2002.
- [4] L. Palumbo et al., "Evaluation of the intra-and inter-method agreement of brain MRI segmentation software packages: A comparison between SPM12 and FreeSurfer v6. 0," *Physica Medica*, vol. 64, pp. 261-272, 2019.
- [5] S. D. Serai, J. Dudley, and J. L. Leach, "Comparison of whole brain segmentation and volume estimation in children and young adults using SPM and SyMRI," *Clinical imaging*, vol. 57, pp. 77-82, 2019.
- [6] E. E. Galletta et al., "Use of computational modeling to inform tDCS electrode montages for the promotion of language recovery in post-stroke aphasia," *Brain Stimulation*, vol. 8, no. 6, pp. 1108-1115, 2015.
- [7] A. Terraneo, L. Leggio, M. Saladini, M. Ermani, A. Bonci, and L. Gallimberti, "Transcranial magnetic stimulation of dorsolateral prefrontal cortex reduces cocaine use: a pilot study," *European Neuropsychopharmacology*, vol. 26, no. 1, pp. 37-44, 2016.

- [8] S. Wortman-Jutt and D. J. Edwards, "Transcranial direct current stimulation in poststroke aphasia recovery," *Stroke*, vol. 48, no. 3, pp. 820-826, 2017.
- [9] A. Pruski and P. Celnik, "The Use of Noninvasive Brain Stimulation, Specifically Transcranial Direct Current Stimulation After Stroke," *American journal of physical medicine & rehabilitation*, vol. 98, no. 8, pp. 735-736, 2019.
- [10] M. Bikson, A. Rahman, and A. Datta, "Computational models of transcranial direct current stimulation," *Clinical EEG and neuroscience*, vol. 43, no. 3, pp. 176-183, 2012.
- [11] I. Laakso, S. Tanaka, M. Mikkonen, S. Koyama, N. Sadato, and A. Hirata, "Electric fields of motor and frontal tDCS in a standard brain space: a computer simulation study," *Neuroimage*, vol. 137, pp. 140-151, 2016.
- [12] P. C. Miranda, M. A. Callejón-Leblic, R. Salvador, and G. Ruffini, "Realistic modeling of transcranial current stimulation: The electric field in the brain," *Current Opinion in Biomedical Engineering*, vol. 8, pp. 20-27, 2018.
- [13] P. Minhas, M. Bikson, A. J. Woods, A. R. Rosen, and S. K. Kessler, "Transcranial direct current stimulation in pediatric brain: a computational modeling study," in *2012 Annual International Conference of the IEEE Engineering in Medicine and Biology Society*, 2012, pp. 859-862: IEEE.
- [14] D. Q. Truong, G. Magerowski, G. L. Blackburn, M. Bikson, and M. Alonso-Alonso, "Computational modeling of transcranial direct current stimulation (tDCS) in obesity: impact of head fat and dose guidelines," *NeuroImage: Clinical*, vol. 2, pp. 759-766, 2013.
- [15] SPM is available at: <https://www.fil.ion.ucl.ac.uk/spm/software/spm12>
- [16] Y. Huang, J. P. Dmochowski, Y. Su, A. Datta, C. Rorden, and L. C. Parra, "Automated MRI segmentation for individualized modeling of current flow in the human head," *Journal of neural engineering*, vol. 10, no. 6, p. 066004, 2013..
- [17] A. K. Boyat and B. K. Joshi, "A review paper: noise models in digital image processing," *arXiv preprint arXiv:1505.03489*, 2015.
- [18] S. Vaishali, K. K. Rao, and G. S. Rao, "A review on noise reduction methods for brain MRI images," in *2015 International Conference on Signal Processing and Communication Engineering Systems*, 2015, pp. 363-365: IEEE.
- [19] M. Aksam Iftikhar, A. Jalil, S. Rathore, and M. Hussain, "Robust brain MRI denoising and segmentation using enhanced non - local means algorithm," *International Journal of Imaging Systems and Technology*, vol. 24, no. 1, pp. 52-66, 2014.
- [20] The denoising toolbox is available at: <https://sites.google.com/site/pierrickcoupe/software/denoising-for-medical-imaging/mri-denoising/mri-denoising-software>
- [21] J. V. Manjón, P. Coupé, A. Buades, D. L. Collins, and M. Robles, "New methods for MRI denoising based on sparseness and self-similarity," *Medical image analysis*, vol. 16, no. 1, pp. 18-27, 2012.
- [22] The used data is available at: <http://insight-journal.org/midas/community/view/21>
- [23] E. Bullitt et al., "Vessel tortuosity and brain tumor malignancy: a blinded study1," *Academic radiology*, vol. 12, no. 10, pp. 1232-1240, 2005.